Negative pressure induced ferroelectric phase transition in rutile TiO_2

2009 J. Phys.: Condens. Matter 21 275901

(http://iopscience.iop.org/0953-8984/21/27/275901)

J. Phys.: Condens. Matter **21** (2009) 275901 (6pp) doi:10.1088/0953-8984/21/27/275901

Negative pressure induced ferroelectric phase transition in rutile TiO_2

Yong Liu[1,2], Lihong Ni[1], Zhaohui Ren[1], Gang Xu[1], Chenlu Song[1,3] and Gaorong Han[1]

[1] State Key Laboratory of Silicon Materials, Department of Materials Science and Engineering, Zhejiang University, Hangzhou 310027, People's Republic of China
[2] Angstrom Center, Institute of Science and Technology, Zhejiang University, Hangzhou 310027, People's Republic of China

E-mail: songcl@zju.edu.cn

Received 9 December 2008, in final form 24 May 2009
Published 12 June 2009
Online at stacks.iop.org/JPhysCM/21/275901

Abstract

First-principles pseudopotential calculations by means of the local density approximation (LDA) within density-functional theory (DFT) are carried out to investigate the negative pressure induced ferroelectric phase transition in rutile TiO_2 in the range of −25 to 25 GPa. The softening behavior of the A_{2u}(TO) modes at the Γ point following the decreasing pressure leads to a ferroelectric phase transition from $P4_2/mnm$ (rutile) space group to $P42nm$ (*ferro*) space group. The calculated pressure dependence of the phonon frequencies, A_1(TO), E(TO), and B_2 modes of the *ferro* TiO_2 relative to A_{2u}(TO), E_u(TO), and B_{1u} modes of rutile TiO_2, indicates that the phase transition occurs at around −10 GPa, consistent with the total energy results. The dramatic increase of the *c*-axial dielectric tensor in the vicinity of the phase transition indicates it to be a typical ferroelectric phase transition. The character of the phase transition is generally identified in terms of the calculated order parameters, displaying a second order.

(Some figures in this article are in colour only in the electronic version)

1. Introduction

Titanium dioxide (TiO_2) is of great importance in both fundamental research and technical applications, exhibiting high photon-to-electron conversion efficiencies [1], reactivity photocatalysis [2], and large dielectric constants [3]. Besides naturally existent polymorphic forms, including rutile, anatase, and brookite phases, a series of new high pressure structured TiO_2 with interesting properties is obtained at elevated pressures. For instance, a high pressure phase TiO_2 with cotunnite structure (c-TiO_2) appears as the hardest oxide ever known, which is synthesized under pressures over 60 GPa and temperatures over 1000 K [4].

A large amount of experimental and theoretical work has been done, focusing on the high pressure induced phase transition of TiO_2. The transformations from the anatase to the columbite and baddeleyite phases have been detected under 2.6–8 GPa and 13–17 GPa respectively with Raman spectroscopy and x-ray diffraction [5, 6]. Using first-principles calculations, Sasaki [7] has indicated that the rutile–columbite–baddeleyite phase transition occurs energetically at 7.5 and 26 GPa, respectively, while Muscat *et al* [8] have shown that the computed anatase–columbite, rutile–columbite, columbite–baddeleyite, and baddeleyite–cotunnite phase transitions appear energetically at about 3.5, 21, 31, and 63 GPa, respectively. These results give a very good insight into the high pressure induced phase transition linking these TiO_2 polymorphs together.

Rutile TiO_2 is also classified to be an incipient ferroelectric, which behaves as a ferroelectric material in its paraelectric phase and shows a rapid increase of the dielectric constant along the *c* axis following the decrease of temperature. However, even when the temperature reaches 0 K the ferroelectric transition does not occur [9]. Montanari *et al* [10] performed a plane-wave pseudopotential implementation of the density function within the framework of the local density approximation on rutile TiO_2, showing that under negative pressure or uniaxial strain a ferroelectric phase transition will occur. However, the sequential TiO_2 ferroelectric phase has not been characterized.

[3] Author to whom any correspondence should be addressed.

Table 1. Fully relaxed structural parameters for rutile and *ferro* TiO_2.

	V	a	c	u	v ($\times 10^4$)
Rutile (present)	59.9614	4.5344	2.9163	0.303 788	
Rutile (calc.) [10]	60.4779	4.551	2.920	0.3040	
Rutile (calc.) [14]	61.1887	4.5672	2.9334	0.3038	
Rutile (exp.) [15]	62.3616	4.59	2.96	0.306	
Ferro (present)	59.9673	4.5347	2.9162	0.303 758	6.1554

In the present paper, we focus on the negative pressure induced ferroelectric phase transition in rutile TiO_2. The density-functional theory (DFT) calculations within the local density approximation (LDA) were performed to study the pressure dependence of the TiO_2 structure and the corresponding properties. The TiO_2 ferroelectric phase was characterized. We also identified the character of the ferroelectric phase transition. In practice, the application of negative hydrostatic pressure is challenging. However, it has been shown that in-plane tensile stress occurring in epitaxial films is not only able to adjust Curie temperature but also able to change an incipient ferroelectric, for instance $SrTiO_3$, to a true ferroelectric [23]. Thus the followed theoretical studies about the effect of negative pressures are very useful for better understanding of the structural instability of TiO_2 and possibly provide an avenue to obtain ferroelectrics from incipient materials.

2. Method

A first-principles density-functional theory (DFT) within the local density approximation (LDA) was employed to perform the theoretical investigation. The extended norm-conserving pseudopotentials including more states as semi-core than in the Troullier–Martins' were used for all atoms [11], considering Ti(3s, 3p, 3d, 4s) and O(2s, 2p) orbits expended using plane waves with a cutoff energy of 55 Hartree. A $6 \times 6 \times 8$ Monkhorst–Pack mesh was employed to perform the integration in the reciprocal space. These parameters were tested and showed enough convergence for the energy calculation. The convergence of the structural optimizations requires the Hellmann–Feynman forces to be less than 10^{-6} hartree/bohr ($\approx 5 \times 10^{-5}$ eV Å^{-1}). The phonon frequencies and the dielectric tensors of TiO_2 were calculated based on the density-functional perturbation theory (DFPT) [12].

All of these simulations are performed by using the *ABINIT* software package [13] at cluster *Lenovo 1800*.

3. Results

3.1. Isotropic pressure dependence of structural stability for rutile TiO_2

The fully optimized structure parameters for rutile TiO_2 are listed in table 1. The theoretical lattice constants are smaller than the experimental values due to the LDA's character, but the differences are less than 1.5%. The resident pressures of the unit cell with optimized lattice constants are less than 1×10^{-4} GPa, which is sufficiently small for the practical calculations related to the phonon properties. The calculated phonon frequencies at the Γ point of rutile TiO_2 are shown in table 2. The experimental neutron scattering [19], infrared and Raman [20, 21] and other calculated results are also listed. The present results have a good agreement with the experimental and theoretical values; the deviation from other calculations is less than ~ 10 cm^{-1}.

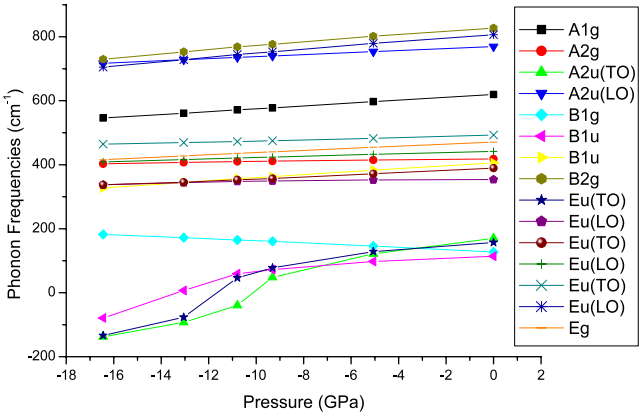

Figure 1. Calculated phonon frequencies at the Γ point of rutile TiO_2 as a function of pressure.

Table 2. Calculated phonon frequencies at Γ point for rutile and *ferro* TiO_2 with fully relaxed structural parameters.

Rutile	Rutile (present)	Rutile (calc.) [18]	Rutile (exp.) [20, 21]	*Ferro*	
B_{1u}	113.9774	116.7	113 [19]	B_2	113.8058
B_{1g}	127.0661	125.2	143	B_1	127.2529
E_u(TO)	157.0934	164.8	183	E(TO)	157.1486
A_{2u}(TO)	169.8428	176.1	167	A_1(TO)	169.3745
E_u(LO)	353.5886	351.5	373	E(LO)	353.6248
E_u(TO)	389.5581	391.3	388	E(TO)	389.5850
B_{1u}	405.5413	407.5	406 [19]	B_2	405.2915
A_{2g}	417.917	415.5		A_2	417.9510
E_u(LO)	441.4259	441.7	458	E(LO)	441.4318
E_g	470.9252	471.5	447	E(TO)	470.6107
				E(LO)	470.7439
E_u(TO)	492.8863	492.8	500	E(TO)	492.9528
A_{1g}	619.3465	622.5	612	A_1(TO)	619.0701
				A_1(LO)	619.0888
A_{2u}(LO)	769.2788	769.3	812	A_1(LO)	769.0187
E_u(TO)	806.4344	808.4	807	E(LO)	806.4271
B_{2g}	827.0474	828.0	827	B_2	826.9440

Starting from the fully relaxed structure, the phonon frequencies at the Γ point are calculated as a function of negative pressure as shown in figure 1. Except for the B_{1g} mode, all the vibration modes become softer as pressure decreases. The B_{2g}, E_u(LO), and A_{2u}(LO) are the three stiffest modes, while the A_{2u}(TO), E_u(TO), and B_{1u} are the three softest modes and become negative values at about -10 GPa, -11.5 GPa, and -13 GPa, respectively. These trends have a good agreement with Montanari's results [10], which, however, predict that the instability occurs at around -4 GPa. The present calculations confirm the previous prediction that rutile TiO_2 becomes unstable with the softening of the A_{2u} modes.

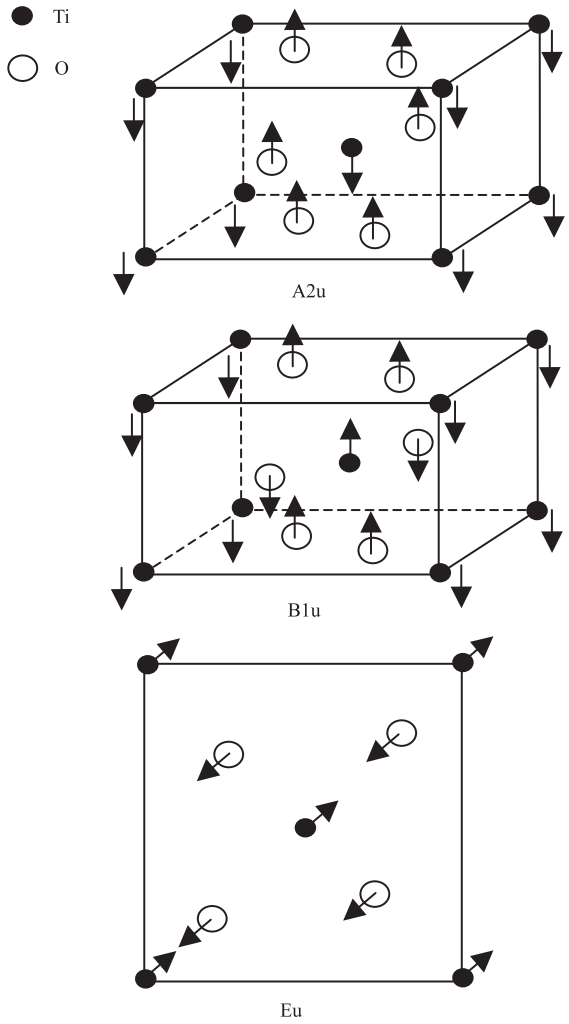

Figure 2. Schematic image of atomic displacements associated with the A_{2u}(TO), E_u(TO), and B_{1u} modes.

The atomic displacements associated with the A_{2u}(TO), B_{1u}, and E_u(TO) modes are schematically shown in figure 2. The softest A_{2u} mode involves a rigid displacement of the Ti sublattice along the *c*-axis and an analogous displacement of the O sublattice but with an opposite sign. This displacement will change TiO_2 from the $P4_2/mnm$ (D_{4h}) space group to the $P42nm$ (C_{4v}) space group. The atomic displacements associated with the B_{1u} modes involve relative displacements of apical Ti and center Ti atoms and those of external and internal O atoms, changing rutile TiO_2 into the $P\bar{4}21m$ (D^3_{2D}) space group. The atomic displacements with the E_u modes involve similar displacements with the A_{2u}(TO) modes, except they move along the ⟨110⟩ direction, changing rutile TiO_2 into the Pm (C_s) space group. The sequential phases corresponding to the A_{2u} and E_u modes are possibly ferroelectric while the sequential phase corresponding to B_{1u} is paraelectric. In this paper, we only pay attention to the ferroelectric phase of TiO_2 related to the A_{2u}(TO) modes, referring to it as *ferro* phase in the following sections.

3.2. Pressure induced phase transition from rutile to ferro TiO_2

The *ferro* TiO_2 is characterized by the tetragonal space group $P42nm$. The unit cell contains two TiO_2 units with Ti ions at 2a Wyckoff positions $(0, 0, v)$ and $(1/2, 1/2, v + 1/2)$ and O ions at 4c Wyckoff positions (u, u, z), $(-u, -u, v)$, $(-u+1/2, u+1/2, v+1/2)$, $(u+1/2, -u+1/2, v+1/2)$. Fully optimized structural parameters and corresponding phonon frequencies are calculated, as shown in tables 1 and 2, respectively. It is found that the lattice constants of the *ferro* TiO_2 are very close to the values of rutile TiO_2, as well as the phonon frequencies. In fact, the difference of the corresponding phonon frequencies shown in table 2 is $\sim$1 cm^{-1}. Note that, from the factor group analysis for the *ferro* primitive cell, the optical modes at the Γ point are classified into the following symmetry species:

$$\Gamma_{opt} = 2A_1 + A_2 + B_1 + 3B_2 + 4E. \quad (1)$$

The cohesive energies as a function of unit cell volume corresponding to restrict relaxed structural parameters (fixing the unit cell volume) are calculated as shown in figure 3(a), and the volume expandabilities as a function of pressure for rutile and *ferro* TiO_2 are shown in figure 3(b). The bulk modulus of rutile and *ferro* TiO_2 are predicted from the curves to be $B = 250.2$ and 243.9 GPa, in agreement with the experimental values of 230 ± 20 GPa [16, 17]. However, under negative pressure the *ferro* TiO_2 is more energetically stable and compressible than rutile TiO_2, consistent with the fact that the ferroelectricity favors the more compressible structure and larger volume. Using the curves in figure 3, the rutile-to-*ferro* transition pressure at $T = 0$ K can be predicated by the enthalpy difference with the following equation:

$$\Delta H_{f-r} = \Delta E_{f-r} + \Delta V_{f-r} \times P \quad (2)$$

where H and E are the enthalpy and total energy of the unit cell; the subscripts f and r refer to the *ferro* and rutile TiO_2 respectively. Because of the very small enthalpy difference between the *ferro* and rutile as shown in figure 4, the calculated phase transition pressure needs to be examined by directly studying energy derivative properties, such as phonon frequencies and dielectric constants. The calculated pressure dependences of the phonon frequencies at the Γ point and the dielectric tensor along the *c* direction in the *ferro* TiO_2 are shown in figures 5 and 6, respectively. It can be found that the three lowest A_1(TO), E(TO), and B_2 modes, which are related to the A_{2u}(TO), E_u(TO), and B_{1u} modes in rutile TiO_2 respectively, exhibit softening behaviors until the pressure decreases to −10 GPa, and then become stiffer as the pressure decreases further. Other phonon modes, such as E(LO) at 441 cm^{-1}, E(TO) at 470 cm^{-1}, E(TO) at 492 cm^{-1}, and A_1(LO) at 619 cm^{-1}, also show abrupt changes at around −10 GPa. The calculated *c*-axis dielectric tensor shows a dramatic increase at around −10 GPa, more than sixfold compared with the values at zero pressure, implying that this process is a typical ferroelectric phase transition. The estimated phase transition pressure, −10 GPa, agrees well with the total energy results (figure 4).

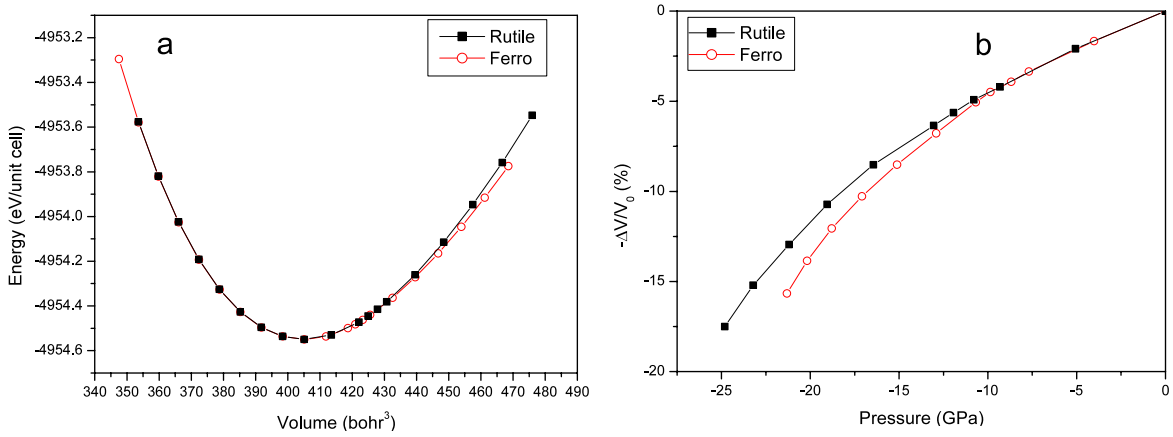

Figure 3. Cohesive energy as a function of unit cell volume (a) and volume expandability as a function of pressure (b) for rutile and *ferro* TiO_2.

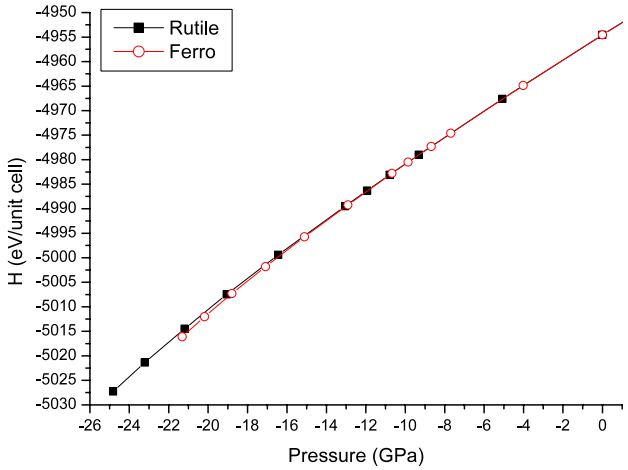

Figure 4. Calculated enthalpy as a function of pressure for rutile and *ferro* TiO_2.

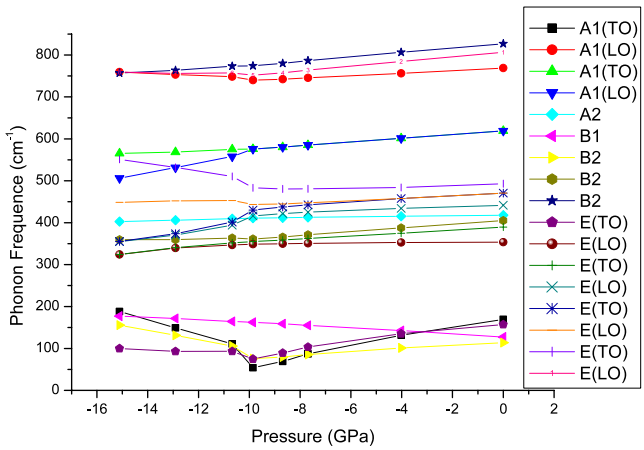

Figure 5. Calculated phonon frequencies at the Γ point of *ferro* TiO_2 as a function of pressure.

3.3. Characteristics of the ferroelectric phase transition

For the purpose of investigating the characteristics of the ferroelectric rutile-to-*ferro* phase transition in TiO_2, further calculations have been performed to generate the pressure

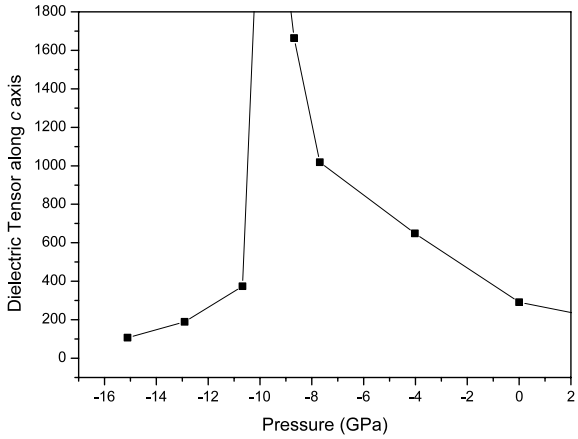

Figure 6. Calculated dielectric tensor along the *c* axis in the vicinity of the phase transition.

dependence of the unit cell volume, spontaneous polarization P_s and structural parameter v, as shown in figure 7. Assuming the crystal is purely ionic by neglecting the electronic polarization, P_s can be obtained from $P_s = \sum_i q_i v_i / V$, where q_i is the ionic charge of the ith atom. Although the Born effective charges need to be used to obtain an accurate value of spontaneous polarization, it is acceptable to employ the ionic charges since we focus on the relative values only.

All of the volume, P_s and v show continuous decreases towards to zero, with P_s and v reaching zero corresponding to the paraelectric rutile TiO_2 at around -10 GPa. This continuous behavior proves a second-order character of the phase transition. Noticeably, the value of P_s under the pressure -15 GPa is nearly 20 μC cm^{-2} and increases to nearly 40 μC cm^{-2} at -20 GPa. These values are close to the theoretical results for ferroelectric $PbTiO_3$ calculated in the same way [22], which implies a possibility of negative pressure induced *ferro* TiO_2 in application.

4. Conclusions and discussion

The negative pressure induced rutile-to-*ferro* phase transition in TiO_2 has been investigated by using the DFT-LDA method.

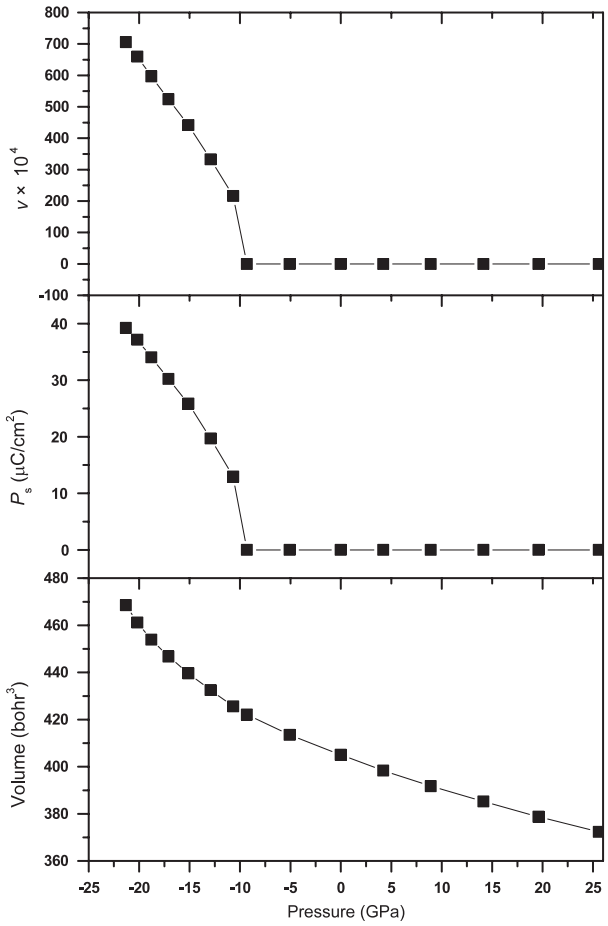

Figure 7. Volume of unit cell, P_s, and v as function of pressure.

The three softest phonon modes, A_{2u}(TO), E_u(TO), and B_{1u} of rutile TiO_2 become negative at −10 GPa, −11.5 GPa, and −13 GPa, respectively, which means that the rutile structure is unstable at −10 GPa and the phase transition is related to the softening behavior of the A_{2u}(TO) mode as the pressure decreases. The sequential phase TiO_2 belongs to $P42nm$ space group and the spontaneous polarization is along the c axis. The calculated bulk modulus under zero pressure of the *ferro* TiO_2, 243.9 GPa, is slightly smaller than the value of rutile TiO_2, 250.2 GPa. The values of the structural constants and the phonon frequencies of rutile and the *ferro* TiO_2 under zero pressure are very close. But under the negative pressure, the *ferro* phase behaves as much softer, consist with the fact that the ferroelectricity favors the more compressible structure. The pressure dependences of unit cell volume, spontaneous polarization P_s, and structural parameter v exhibit a continuous decrease toward zero and P_s and v do become zero at around −10 GPa, evidencing a second-order character of the phase transition, and the transition pressure is −10 GPa.

It is worthwhile to note that we assume that the ferroelectric phase transition of TiO_2 is purely displacive instead of order–disorder. $BaTiO_3$, however, which has a similar crystal structure to rutile TiO_2, exhibits a complicated case in that it is intermediate between order–disorder and displacive nature. This is because the centro-symmetry of Ti in the TiO_6 octahedron is not stable due to the pseudo-Jahn–Teller effects (PJTE) leading into dipole-moment formation in its high temperature phases and being partly ordered at low temperature. This was shown theoretically and experimentally almost 30 years ago [25–27]. Although to the authors' knowledge no experimental or theoretical investigations have been done to prove that rutile TiO_2 is completely or partially ordered corresponding to PJTE and the uncertainty of the choice of the purely displacive nature still remains, we believe that rutile TiO_2 favors the displacive nature because its PJTE is weaker than that in $BaTiO_3$. To elucidate this issue we rewrite equation (5.30) in Bersuker's book [24] as the following:

$$4F^2/K\Delta - 1 > 0 \tag{3}$$

where Δ is the half energy gap between the ground and excited states under consideration, which are mixed by T_{1u} displacements, F is the vibronic constant, and K is the force constant of the T_{1u} vibrations. The greater the left part, the deeper the adiabatic potential, and the higher the temperature of phase transition to the paraphase, which means stronger PJTE. Considering the series of $SrTiO_3$, TiO_2, and $BaTiO_3$, the Ti–O distance increases from 1.95 to 1.98 Å, then to 2.01 Å. Consequently, the force constant K and the effective energy distance between the bands decrease while the vibronic constant F is less influenced. Thus from $SrTiO_3$, to TiO_2, then to $BaTiO_3$, the PJTE is strengthened and the conditions of ferroelectricity occurrence are improved. This trend is consistent with the fact that both $SrTiO_3$ and rutile TiO_2 are incipient ferroelectrics but $BaTiO_3$ is a true one. For weak PJTE the ground state is softened but remains stable, which implies there is no (local) dipolar moment in the paraphase and the transition is not order–disorder but displacive. Furthermore, the PJTE in rutile TiO_2 is much stronger than that in $SrTiO_3$. Since in-plane tensile strains can change $SrTiO_3$ to true ferroelectricity in epitaxial films [23], less tensile strain will act on TiO_2. This adds further validity to the present theoretical investigations.

Acknowledgment

The authors would like to thank Zhejiang University National Science Park for the technical support provided during the period of this research.

References

[1] Bach U, Lupo D, Comte P, Moser J E, Weissörtel F, Salbeck J, Spreitzer H and Grätzel M 1998 *Nature* **395** 583
[2] Asahi R, Morikawa T, Ohwaki T, Aoki K and Taga Y 2001 *Science* **293** 269
[3] Gan J Y, Chang Y C and Wu T B 1998 *Appl. Phys. Lett.* **72** 332
[4] Dubrovinsky L S, Dubrovinskaia N A, Swamy V, Muscat J, Harrison N M, Ahuja R, Holm B and Johansson B 2001 *Nature* **410** 653
[5] Haines J and Léger J M 1993 *Physica* B **192** 233
[6] Lagarec K and Desgreniers S 1995 *Solid State Commun.* **94** 519
[7] Sasaki T 2002 *J. Phys.: Condens. Matter* **14** 10557
[8] Muscat J, Swamy V and Harrison N M 2002 *Phys. Rev.* B **65** 224112
[9] Parker R A 1961 *Phys. Rev.* B **124** 1719

[10] Montanari B and Harrison N M 2004 *J. Phys.: Condens. Matter* **16** 273
[11] Troullier N and Martins J L 1991 *Phys. Rev.* B **43** 1993
[12] Hamann D R, Wu X, Rabe K M and Vanderbilt D 2005 *Phys. Rev.* B **71** 035117
[13] Gonze X, Beuken J M, Caracas R, Detraux F, Fuchs M, Rignanese G M, Sindic L, Verstraete M, Zerah G, Jollet F, Torrent M, Roy A, Mikami M, Ghosez Ph, Raty A and Allan D C 2002 *Comput. Mater. Sci.* **25** 478
[14] Sikora R 2005 *J. Phys. Chem. Solids* **66** 1069
[15] Gervais F and Kress W 1985 *Phys. Rev.* B **31** 4809
[16] Isaak D G, Carnes J D, Anderson O L, Cynn H and Hake E 1998 *Phys. Chem. Miner.* **26** 31
[17] Gerward L and Olsen J S 2007 *J. Appl. Crystallogr.* **30** 259
[18] Lee C, Ghosez Ph and Gonze X 1994 *Phys. Rev.* B **50** 13379
[19] Traylor J G, Smith H G, Nicklow R M and Wilkinson M K 1971 *Phys. Rev.* B **3** 3457
[20] Porto S P S, Fleury P A and Damen T C 1967 *Phys. Rev.* **154** 522
[21] Eagles D M 1964 *J. Phys. Chem. Solids* **25** 1243
[22] Liu Y, Ni L H, Xu G, Song C L, Han G R and Zheng Y 2008 *Physica* B **403** 3863
[23] Haenl J H, Irvin P, Chang W, Uecker R, Reiche P, Li Y L, Choudhury S, Tian W, Hawley M E, Craigo B, Tagantsev A K, Pan X Q, Streiffer S K, Chen L Q, Kirchoefer S W, Levy J and Schlom D G 2004 *Nature* **430** 758
[24] Bersuker I B 1984 *The Jahn–Teller Effect and Vibronic Interactions in Modern Chemistry* (New York: Plenum)
[25] Bersuker I B 1966 *Phys. Lett.* **20** 589
[26] Comes R, Lambert M and Guinier A 1968 *Solid State Commun.* **6** 715
[27] Lambert M and Comes R 1969 *Solid State Commun.* **7** 305